

ANOMALY MEDIATED SUPERSYMMETRY BREAKING AND ITS TEST IN LINEAR COLLIDERS

SOUROV ROY

*Helsinki Institute of Physics, P.O. Box 64
 FIN-00014 University of Helsinki, Finland
 roy@pcu.helsinki.fi*

Signatures of anomaly mediated supersymmetry breaking in linear colliders are briefly reviewed after presenting an outline of the theoretical framework. A unique and distinct feature of a large class of models of this type is a winolike chargino which is very closely degenerate in mass with the lightest neutralino. The very slow decay of this chargino results in a heavily ionizing charged track and one soft charged pion with a characteristic momentum distribution, leading to unique signals in linear colliders which are essentially free of background. The determination of chargino and slepton masses from such events is a distinctly interesting possibility.

Keywords: Supersymmetry breaking; Linear Collider.

PACS Nos.: 12.60.Jv, 14.80.Ly

1. Introduction

The Minimal Supersymmetric Standard Model (MSSM), with softly broken $N=1$ supersymmetry (SUSY) is perhaps the most well-motivated theory for physics beyond the Standard Model (SM). The question then arises as to how SUSY is broken and why is the mechanism of SUSY breaking relevant to experiments. The most general version of the MSSM, containing a large number of arbitrary SUSY breaking soft parameters, is somewhat intractable from the viewpoint of experimental searches. However, if the mechanism of SUSY breaking and the way SUSY breaking is communicated to the MSSM superfields were known, then it would be possible to have a much smaller set of parameters. The nature of the lightest supersymmetric particle (LSP) and the decay chains could then be established from the prediction of mass spectra and couplings from the framework underlying SUSY breaking. Hence, the theorist's approach would be to understand the origin of these parameters in terms of some kind of spontaneous SUSY breaking.

It had been realized¹ that if spontaneous SUSY breaking arose from MSSM fields themselves then the spectrum should obey certain sum rules, namely $STrM_d^2 + ST rM_u^2 = 0 = ST rM_e^2 + ST rM_\nu^2$, generation by generation. This implies that in every family at least some sleptons/squarks must be lighter than their partner leptons/quarks, contrary to observation. However, this equation holds only for renor-

malizable theories and at tree level. Thus, in order to avoid this situation one can imagine that SUSY is broken dynamically in some ‘hidden’ sector which is singlet under the SM interactions and then the message of SUSY breaking is communicated to the ‘visible’ sector of MSSM fields through some mediation mechanisms which involve either loops or non-renormalizable interactions. The nature of the soft SUSY breaking in the visible sector is thus determined by the mediation mechanism of SUSY breaking.

Several such mediation mechanisms have been discussed in the literature, such as supergravitational mediation at the tree level² and gauge mediation³, along with their distinctive phenomenological signatures. Anomaly mediated supersymmetry breaking (AMSB)^{4,5} is one such possibility and has attracted a lot of attention in recent times. The basic idea is to convey the message of supersymmetry breaking to the observable sector by the Super-Weyl anomaly. This scenario has led to the construction of a whole class of models^{6,7,8,9,10,11,12,13,14,15,16,17,18,19,20,21,22,23} and many of the phenomenological implications have been discussed^{8,24,25,26,27,28,29,30,31,32,33,34,35,36,37,38,39,40}. For example, the characteristic signatures of the minimal anomaly mediated supersymmetry breaking (mAMSB) model have been studied in the context of hadronic colliders^{25,26,27,28,29,30,31,32,33}, as well as for high energy linear colliders, whether of the e^+e^- type^{34,35,36,37,38}, or $e^-\gamma$ colliders³⁹ or photon-photon colliders⁴⁰. In this article we will briefly review the unique signatures of the mAMSB model in the context of high energy linear colliders.

The original version of the AMSB scenario involved a higher-dimensional supergravity theory where the hidden sector and observable sector superfields are localized on two distinct parallel three-branes separated by a distance $\sim r_c$ (r_c is the compactification radius) in the extra dimension.⁴ As there is no tree level coupling between the hidden sector fields and those in the observable sector, it had been assumed that the flavor changing neutral current (FCNC) processes would be suppressed naturally. Recently, though, it has been shown that the physical separation between the visible and hidden sectors in extra dimension is not sufficient to suppress the FCNC processes except in some special cases.¹⁹ However, it is possible to construct models of AMSB, even in a completely four-dimensional framework, that can circumvent the flavour problem.^{20,21} For the purposes of the present review, we would be concentrating on the minimal scenario of Ref. ⁴.

The AMSB scenario can be described in terms of a four-dimensional effective theory below the compactification scale, $\mu_c(\sim r_c^{-1})$ where only four-dimensional supergravity fields are assumed to propagate in the bulk. It is then possible to define a rescaling transformation which can eliminate, from the classical Lagrangian, any tree-level interaction (except for the μ -term in the superpotential) connecting the supergravity fields with the visible sector matter fields. Such a rescaling transformation, however, is anomalous at the quantum level and hence supersymmetry breaking is communicated from the hidden sector to the visible sector through the loop-generated super-conformal anomaly.⁴ The supersymmetry breaking soft mass

parameters for the gauginos and the scalars are generated at the same order in the corresponding gauge coupling strength. The analytical expressions for the scalar and gaugino masses, in terms of the supersymmetry breaking parameters, are renormalization group (RG) invariant, and, thus, can be computed at the low-energy scale in terms of the appropriate beta functions and anomalous dimensions. However, at low energies, it predicts the existence of tachyonic sleptons. This is the most glaring problem of the minimal AMSB scenario. Several solutions to this problem exist. In this review we shall consider mainly the minimal AMSB model wherein a constant term m_0^2 is added to all the scalar squared masses thereby making the slepton mass-squareds sufficiently positive. While this may seem to be an *ad hoc* step, models have been constructed¹⁶ that naturally lead to such an eventuality. A consequence is that the RG invariance of the expression for scalar masses is lost and hence one needs to consider the corresponding evolution down to the electroweak scale.

The minimal AMSB model has several unique features. The gravitino is very heavy, its mass being in the range of tens of TeV. Left and right selectrons and smuons are nearly mass-degenerate while the staus split into two distinct mass eigenstates. But perhaps the most striking feature is that both the lightest supersymmetric particle (LSP) $\tilde{\chi}_1^0$ and the lighter chargino ($\tilde{\chi}_1^\pm$) are predominantly Winos and hence nearly mass-degenerate. Loop corrections as well as a small gaugino-Higgsino mixing at the tree level do split the two,^{26,41} but the consequent mass difference is very small: $\Delta M < 1\text{GeV}$. The dominant decay mode of the lighter chargino is $\tilde{\chi}_1^\pm \rightarrow \tilde{\chi}_1^0 + \pi^\pm$ and this long-lived chargino would typically result in a heavily ionizing charged track and/or a characteristic soft pion in the detector.⁴²

The review is organized as follows. In Sec.2 we discuss the spectra in the mAMSB scenario and constraints on the parameter space coming from various experimental and theoretical considerations. In Sec.3, we first mention the results of the experimental searches of mAMSB scenario at LEP and then go on to discuss the signatures of mAMSB scenario in the context of a high energy e^+e^- linear collider. Next, in Sec.4 we discuss the potential of an $e^-\gamma$ collider and $\gamma\gamma$ collider in order to look for the signatures of AMSB. Finally, we conclude in Sec.5.

2. Model Parameters and Constraints

The minimal AMSB model is described by just three parameters (apart from the SM parameters, of course): the gravitino mass $m_{3/2}$, the common scalar mass parameter m_0 and $\tan\beta$, the ratio of the two Higgs vacuum expectation values. In addition, there is a discrete variable, namely the sign of the Higgs mass term (μ). As mentioned earlier, the soft supersymmetry breaking terms in the effective Lagrangian are then determined solely in terms of the gauge (g_i) and Yukawa (y_a) couplings.

Denoting the generic beta-functions and anomalous dimension by $\beta_g(g, y) \equiv dg/dt$, $\beta_y(g, y) \equiv dy/dt$ and $\gamma(g, y) \equiv d\ln Z/dt$ (t being the logarithmic scale vari-

able) respectively, we have, for the gaugino (λ) masses

$$M_\lambda = \frac{\beta_g}{g} m_{3/2}, \quad (1)$$

where the appropriate gauge coupling and β -function are to be considered. Similarly, for the trilinear soft breaking parameters, one has

$$A_y = \frac{\beta_y}{y} m_{3/2}. \quad (2)$$

The scalar masses can be symbolically written as,

$$m_{\tilde{f}}^2 = m_0^2 - \frac{1}{4} \sum \left(\frac{\partial \gamma}{\partial g} \beta_g + \frac{\partial \gamma}{\partial y} \beta_y \right) m_{3/2}^2. \quad (3)$$

The detailed expressions for the gaugino masses at the one-loop level and the squared masses for the Higgs and the other scalars at the two-loop level can be found in Refs. ^{26,36,43}. Certain sum rules have also been derived for the sparticle masses in the mAMSB model.⁴⁴

A particularly interesting feature of the mAMSB model is that the ratios of the respective $U(1)$, $SU(2)$ and $SU(3)$ gaugino mass parameters M_1 , M_2 and M_3 , at low energies, turn out to be

$$|M_1| : |M_2| : |M_3| \approx 2.8 : 1 : 7.1. \quad (4)$$

An immediate consequence is that the lighter chargino $\tilde{\chi}_1^\pm$ and the lightest neutralino $\tilde{\chi}_1^0$ are both almost exclusively a Wino and, hence, nearly degenerate in mass. As already discussed in the introduction a small mass difference is generated (the lighter chargino is always the heavier) though from the tree-level gaugino-Higgsino mixing as well as from the one-loop corrected chargino and the neutralino mass matrices.^{26,41} The mass splitting has an approximate form:

$$\begin{aligned} \Delta M \equiv m_{\tilde{\chi}_1^\pm} - m_{\tilde{\chi}_1^0} &= \frac{M_W^4 \tan^2 \theta_W}{(M_1 - M_2) \mu^2} \sin^2 2\beta \left[1 + \mathcal{O} \left(\frac{M_2}{\mu}, \frac{M_W^2}{\mu M_1} \right) \right] \\ &+ \frac{\alpha M_2}{\pi \sin^2 \theta_W} \left[f \left(\frac{M_W^2}{M_2^2} \right) - \cos^2 \theta_W f \left(\frac{M_Z^2}{M_2^2} \right) \right], \end{aligned} \quad (5)$$

with

$$f(x) \equiv -\frac{x}{4} + \frac{x^2}{8} \ln(x) + \frac{1}{2} \left(1 + \frac{x}{2} \right) \sqrt{4x - x^2} \tan^{-1} \left(\frac{(1-x)\sqrt{4x-x^2}}{3x-x^2} \right). \quad (6)$$

For the range of m_0 and $m_{3/2}$ that we would be considering throughout this review, $\Delta M \lesssim 500$ MeV. And, for very large M_2 , the mass difference reaches an asymptotic value of ≈ 165 MeV.

To determine the parameter space allowed to the theory, several experimental constraints need to be considered, the most important ones being:

- $\tilde{\chi}_1^0$ must be the LSP;
- $m_{\tilde{\tau}_1} > 82$ GeV,⁴⁵

- $m_{\tilde{\chi}_1^\pm} > 86$ GeV, when this chargino almost degenerate with the lightest neutralino.⁴⁶

The last constraint serves to rule out relatively low values of $m_{3/2}$ *irrespective* of the value of m_0 . A detailed discussion of these issues can be found in Ref.⁴³.

One must also consider the constraints^{27,43,47,48} on the mAMSB model parameters from the recent measurement of the muon anomalous magnetic moment ($g_\mu - 2$). It must be borne in mind, though, that the calculation of the SM contribution to $(g_\mu - 2)$ is beset with many theoretical uncertainties. Constraints are also derivable^{27,47,48} from the measurement of the rare decay rate $\Gamma(B \rightarrow X_s \gamma)$. Additional bounds may exist if one demands that the electroweak vacuum corresponds to the global minimum of the scalar potential.^{49,50}

3. AMSB Signals at e^+e^- Collider

The search for nearly degenerate lighter chargino and the lightest neutralino (lightest neutralino being the LSP) has been performed by all the four experiments at LEP2 and bounds have been derived on the lighter chargino mass at 95% C.L. from the signal which consists of a single high p_T ISR photon plus a large amount of missing energy.^{46,51,52}

3.1. Signals of AMSB at high energy e^+e^- linear collider

The viability of the channel $e^+e^- \rightarrow \gamma \tilde{\chi}_1^+ \tilde{\chi}_1^-$ has also been studied at the Next Linear Collider (NLC) with $\sqrt{s} = 500$ GeV within the framework of mAMSB models where the energetic photon and missing energy from the neutralinos in the final state have been used to trigger the event.³⁴ It has been shown that with suitably chosen kinematical cuts to reduce the backgrounds one could observe hundreds of background free events with $\mathcal{L} = 50$ fb⁻¹ in a large region of the allowed parameter space. The track length of the decaying chargino and the impact parameter of the soft pion emitted from the decay of the lighter chargino have also been analyzed in order to see whether these characteristics can be used to make the signal background free. The chargino mass can be determined from kinematics and the sneutrino mass can be determined approximately from the cross section and these information could possibly be used to distinguish the mAMSB models from other models of nearly mass-degenerate lighter chargino and lightest neutralino.

One could also look at pair production processes such as $e^+e^- \rightarrow \tilde{e}_L^\pm \tilde{e}_L^\mp, \tilde{e}_R^\pm \tilde{e}_R^\mp, \tilde{e}_L^\pm \tilde{e}_R^\mp, \tilde{\nu} \tilde{\nu}, \tilde{\chi}_1^0 \tilde{\chi}_2^0, \tilde{\chi}_2^0 \tilde{\chi}_2^0$ at a CM energy $\sqrt{s} = 1$ TeV.^{35,36} The signals analyzed comprise multiple fast charged leptons any of which can be used as a trigger plus heavily ionizing charged tracks from the chargino and/or soft charged pions with characteristic momentum distribution plus a large amount of missing energy.

Depending on various parametric choices, the mAMSB sparticle spectrum has been broadly classified into two categories with the following mass orderings (sparticle symbols standing for the sparticle masses):

- Spectrum A: $\tilde{\chi}_1^0 (\approx \tilde{\chi}_1^\pm) < \tilde{\nu} < \tilde{e}_R (\approx \tilde{e}_L) < \tilde{\chi}_2^0$
- Spectrum B: $\tilde{\chi}_1^0 (\approx \tilde{\chi}_1^\pm) < \tilde{\chi}_2^0 < \tilde{\nu} < \tilde{e}_R (\approx \tilde{e}_L)$.

Also, for large values of $\tan\beta$, there exists a region where the mass of $\tilde{\chi}_2^0$ is between that of the lighter stau $\tilde{\tau}_1$ and the first generation sleptons. This variant, which we call Spectrum B1, is characterized by

- Spectrum B1: $\tilde{\chi}_1^0 (\approx \tilde{\chi}_1^\pm) < \tilde{\tau}_1 < \tilde{\chi}_2^0 < \tilde{\nu} < \tilde{e}_R (\approx \tilde{e}_L)$.

For most of the decay modes, the spectra B and B1 have identical behaviour, the only exception is the decay of $\tilde{\chi}_2^0$, which is discussed in section 3.1.1. Staus and smuons are not considered for production here.

In the next section we shall enumerate all possible decay channels of the low-lying sparticles $\tilde{\chi}_1^\pm$, $\tilde{\chi}_2^0$, \tilde{e}_L , \tilde{e}_R and $\tilde{\nu}$ that result in one or more leptons plus at least one soft charged pion accompanied by missing energy. The selection criteria and conventions can be found in Ref. ³⁶.

3.1.1. *Decay cascade and production processes for spectrum A and spectrum B*

For Spectrum A, the allowed decay channels are as follows:

- (1) $\tilde{\chi}_2^0 \rightarrow \nu\tilde{\nu}, \quad \ell_L^\pm \tilde{\ell}_L^\mp, \quad \ell_R^\pm \tilde{\ell}_R^\mp$.
- (2) $\tilde{e}_L \rightarrow e\tilde{\chi}_1^0, \quad \nu_e \tilde{\chi}_1^\pm$.
- (3) $\tilde{e}_R \rightarrow e\tilde{\chi}_2^{0*} \rightarrow e\nu\tilde{\nu}$. Note that \tilde{e}_R must have a three-body decay since $\tilde{\chi}_1^0$ has a vanishing bino component. Also, the virtual $\tilde{\chi}_2^{0*}$ goes into the $\nu\tilde{\nu}$ channel rather than the $\ell_L^\pm \tilde{\ell}_L^\mp$ channel since $\tilde{\ell}_L$ is never lighter than \tilde{e}_R in minimal AMSB. However, the $\tau\tilde{\tau}_1$ channel is not considered explicitly since we do not look at final states with τ 's.
- (4) $\tilde{\nu} \rightarrow \nu\tilde{\chi}_1^0, \quad \ell^\mp \tilde{\chi}_1^\pm$.

This immediately predicts the decay cascade for low-lying sparticles. As already pointed out, $\tilde{\chi}_1^\pm$ results in a heavily ionizing charged track X_D and/or a soft charged pion^a. Thus, the end products of various sleptons and $\tilde{\chi}_2^0$ are

- (1) $\tilde{\nu} \rightarrow \ell^\pm \pi^\mp \cancel{E}_T$ (it can have a completely invisible mode $\tilde{\nu} \rightarrow \nu\tilde{\chi}_1^0$ and thus can act as a virtual LSP).
- (2) $\tilde{e}_L \rightarrow e\cancel{E}_T, \quad \pi\cancel{E}_T$.
- (3) $\tilde{e}_R \rightarrow e\cancel{E}_T, \quad e\ell^\pm \pi^\mp \cancel{E}_T$.
- (4) $\tilde{\chi}_2^0 \rightarrow \ell^\pm \pi^\mp \cancel{E}_T, \quad \ell^+ \ell^- \cancel{E}_T, \quad \ell_1^+ \ell_1^- \ell_2^\pm \pi^\mp \cancel{E}_T \quad (\ell_1, \ell_2 = e, \mu)$.

The allowed decay channels for Spectrum B are as follows:

- (1) $\tilde{e}_L \rightarrow e\tilde{\chi}_1^0, \quad e\tilde{\chi}_2^0, \quad \nu_e \tilde{\chi}_1^\pm$.

^aHenceforth π will be used to denote X_D and/or charged soft pion.

- (2) $\tilde{e}_R \rightarrow e\tilde{\chi}_2^0$. Thus \tilde{e}_R has a more prompt decay in spectrum B than in spectrum A.
- (3) $\tilde{\nu} \rightarrow \nu\tilde{\chi}_1^0, \nu\tilde{\chi}_2^0, \ell^\mp\tilde{\chi}_1^\pm$.
- (4) The dominant decay modes of $\tilde{\chi}_2^0$ are: $\tilde{\chi}_2^0 \rightarrow \tilde{\chi}_1^0 h, \tilde{\chi}_2^0 \rightarrow \tilde{\chi}_1^0 Z, \tilde{\chi}_2^0 \rightarrow \tilde{\chi}_1^\pm W^\mp$, where h is the lightest CP-even Higgs scalar.
- For Spectrum B1 (see Section 3.1), the two body channel $\tilde{\chi}_2^0 \rightarrow \tau\tilde{\tau}_1$ opens up, and the branching ratios of all the above-mentioned two-body channels get suppressed.

The decay cascades for sleptons and gauginos are:

- (1) $\tilde{\chi}_2^0 \rightarrow \ell^\pm\pi^\mp\cancel{E}_T, \ell^+\ell^-\cancel{E}_T$. $\tilde{\chi}_2^0$ also has a virtual LSP mode $\tilde{\chi}_2^0 \rightarrow \nu\nu\tilde{\chi}_1^0$. The leptons come from the decay of W and Z ; h decays dominantly into $b\bar{b}$ and $\tau\bar{\tau}$ which we do not discuss here.
- (2) $\tilde{\nu} \rightarrow \ell^\pm\pi^\mp\cancel{E}_T, \ell^+\ell^-\cancel{E}_T$ (and the virtual LSP mode listed for spectrum A).
- (3) $\tilde{e}_L \rightarrow e\cancel{E}_T, \pi\cancel{E}_T, e\ell^+\ell^-\cancel{E}_T, e\ell^\pm\pi^\mp\cancel{E}_T$.
- (4) $\tilde{e}_R \rightarrow e\cancel{E}_T, e\ell^+\ell^-\cancel{E}_T, e\ell^\pm\pi^\mp\cancel{E}_T$.

Table 1. Possible one or multilepton signal with one soft pion. All possible combinations of leptonic flavours are to be taken into account where the flavour is not shown explicitly. This table is taken from Ref.³⁶.

Spectrum	Signals	Parent Channels
A	$e\pi$	$\tilde{\nu}\tilde{\nu}, \tilde{e}_L\tilde{e}_L, \tilde{e}_L\tilde{e}_R, \tilde{\chi}_1^0\tilde{\chi}_2^0, \tilde{\chi}_2^0\tilde{\chi}_2^0$
	$\mu\pi$	$\tilde{\nu}\tilde{\nu}, \tilde{\chi}_1^0\tilde{\chi}_2^0, \tilde{\chi}_2^0\tilde{\chi}_2^0$
	$e e \ell \pi$	$\tilde{e}_R\tilde{e}_R, \tilde{e}_L\tilde{e}_R, \tilde{\chi}_1^0\tilde{\chi}_2^0, \tilde{\chi}_2^0\tilde{\chi}_2^0$
	$\mu \mu \ell \pi$	$\tilde{\chi}_1^0\tilde{\chi}_2^0, \tilde{\chi}_2^0\tilde{\chi}_2^0$
	$\ell_1 \ell_1 \ell_2 \ell_2 \ell_3 \pi$	$\tilde{\chi}_2^0\tilde{\chi}_2^0 (\ell_{1,2,3} = e, \mu)$
B	$e\pi$	$\tilde{\nu}\tilde{\nu}, \tilde{e}_L\tilde{e}_L, \tilde{e}_L\tilde{e}_R, \tilde{\chi}_1^0\tilde{\chi}_2^0, \tilde{\chi}_2^0\tilde{\chi}_2^0$
	$\mu\pi$	$\tilde{\nu}\tilde{\nu}, \tilde{e}_L\tilde{e}_L, \tilde{\chi}_1^0\tilde{\chi}_2^0, \tilde{\chi}_2^0\tilde{\chi}_2^0$
	$e \ell_1 \ell_2 \pi$	$\tilde{e}_R\tilde{e}_R, \tilde{e}_L\tilde{e}_R, \tilde{e}_L\tilde{e}_L, \tilde{\nu}\tilde{\nu}, \tilde{\chi}_2^0\tilde{\chi}_2^0$ ($\ell_{1,2} = e, \mu$)
	$\mu \mu \mu \pi$	$\tilde{\chi}_2^0\tilde{\chi}_2^0, \tilde{\nu}\tilde{\nu}$
	$e e \ell_1 \ell_1 \ell_2 \pi$	$\tilde{e}_L\tilde{e}_L, \tilde{e}_R\tilde{e}_R, \tilde{e}_L\tilde{e}_R (\ell_{1,2} = e, \mu)$

A list of all possible final states and their parent sparticles, as discussed above, for both Spectra A and B, is given in Table 1 for one pion channels. A similar list for two pion channels can be seen in Ref.³⁶. In the next section, we discuss some of the one-pion signals and the dilepton plus dipion signal, in detail, but let us note two key features right at this point.

- One can sometimes have the same signal for Spectrum A or B; however, their sources are different. This means that the production cross-section and different distributions will also vary from one spectrum to the other; this may help discriminate between them. A useful option may be to use one polarized beam

when some of the channels would be altogether ruled out.

- Three charged lepton plus one soft pion ($3\ell 1\pi$) signals are interesting in their own right. Consider the $3\mu 1\pi$ signal. For Spectrum B, two opposite sign muons must have their invariant mass peaked at m_Z , while no such compulsion exists for Spectrum A. This can serve as a useful discriminator between these two options. A discussion regarding additional features can be seen in Ref. ³⁶.

3.1.2. *Some numerical results*

Cross sections for the production of various two-particle combinations have been calculated at an e^+e^- CM energy of 1 TeV for two values of $\tan\beta$, namely, 10 and 30, for $\mu > 0$. These cross sections were multiplied by the appropriate branching fractions of the corresponding decay channels to get the final states described below. The selection cuts used can be found in Ref. ³⁶.

Table 2. Selected parameter points with $\mu > 0$ for computed cross sections.

Spectrum	Parameter Set	m_0 (GeV)	$m_{3/2}$ (TeV)	$\tan\beta$
A	(a)	340	44	10
	(b)	350	42	10
	(c)	360	39	10
	(d)	380	46	30
	(e)	410	44	30
	(f)	450	47	30

Here, we shall display numerical results for only a selected subset of the final states listed in section 3.1.1 and the dilepton plus dipion signal - mainly to get an idea of signal strengths. Specifically, let us choose the final states $e\pi\cancel{E}_T$, $ee\mu\pi\cancel{E}_T$, $ee\pi\pi\cancel{E}_T$. In Table 2, we have selected some AMSB parameter points and in Table 3, numbers for the cross sections in the three channels mentioned above are displayed for spectrum A with the parameter points as selected in Table 2. The individual processes have widely different contributions to these channels because of the fact that their individual production cross sections and branching ratios in the cascade decays are highly parameter-dependent. These signals are essentially background free and the detailed discussion regarding the possible backgrounds can be found in Ref. ³⁶. We can see from table (3) that even in the worst cases of the signal cross-sections one could observe 15850, 3 and 4330 signal events in the $e\pi + \cancel{E}_T$, $ee\mu\pi + \cancel{E}_T$ and $ee\pi\pi + \cancel{E}_T$ channels respectively from Spectrum A assuming an integrated luminosity of 500 fb^{-1} . Similar numbers for spectrum B can be found in Ref. ³⁶.

The kinematic distributions of the final state particles for the $e^\pm + \pi^\mp + \cancel{E}_T$ signal have been studied for the following sample point in the AMSB parameter space corresponding to Spectrum A: $m_{3/2} = 44\text{ TeV}$, $\tan\beta = 30$, $\mu > 0$ and $m_0 = 410\text{ GeV}$. These are shown in Fig.1. The detailed discussions regarding these

Table 3. Some selected signals in Spectrum A for sample choices of parameters in Table 3. The contributions from different sources are also shown in the Table. Here, PS stands for Parameter Set.

Signal	PS	Cross Sections (fb)						Total
		$\tilde{\nu}\tilde{\nu}$	$\tilde{e}_L\tilde{e}_L$	$\tilde{e}_R\tilde{e}_R$	$\tilde{e}_L\tilde{e}_R + \tilde{e}_R\tilde{e}_L$	$\tilde{\chi}_1^0\tilde{\chi}_2^0$	$\tilde{\chi}_2^0\tilde{\chi}_2^0$	
$e\pi + E_T$	<i>a</i>	40.27	46.7	-	0.00029	2.46	0.118	89.54
	<i>b</i>	40.94	45.09	-	0.000121	2.48	0.14	88.65
	<i>c</i>	43.03	44.44	-	2.55×10^{-5}	2.14	0.13	89.74
	<i>d</i>	30.17	31.63	-	3.24×10^{-8}	1.74	0.032	63.57
	<i>e</i>	26.4	24.33	-	0.0	1.35	0.011	52.09
	<i>f</i>	17.28	13.43	-	0.0	0.99	0.003	31.70
$ee\mu\pi + E_T$	<i>a</i>	-	-	1.36×10^{-4}	0.010	1.44	0.159	1.61
	<i>b</i>	-	-	3.65×10^{-4}	0.012	1.32	0.174	1.50
	<i>c</i>	-	-	0.00	0.018	1.19	0.116	1.32
	<i>d</i>	-	-	0.00	2.3×10^{-5}	0.014	0.033	0.047
	<i>e</i>	-	-	0.00	4.15×10^{-5}	0.011	0.008	0.019
	<i>f</i>	-	-	0.00	2.02×10^{-5}	0.006	0.001	0.007
$ee\pi\pi + E_T$	<i>a</i>	24.21	-	-	0.014	-	0.0511	24.27
	<i>b</i>	24.94	-	-	0.016	-	0.0648	25.02
	<i>c</i>	27.66	-	-	0.026	-	0.0604	27.74
	<i>d</i>	16.45	-	-	2.7×10^{-5}	-	0.0119	16.46
	<i>e</i>	14.62	-	-	5.04×10^{-5}	-	0.0044	14.62
	<i>f</i>	8.66	-	-	2.41×10^{-5}	-	0.000972	8.66

distributions can be found in Ref. ³⁶. For these values of AMSB input parameters, $\Delta M = 198$ MeV.

Before going to the next section let us also mention that the possibility of observing same sign dilepton signals induced by the $\tilde{\nu}\tilde{\nu}^*$ mixing in the AMSB model (where $\tilde{\tau}$ is the LSP) has been discussed in Ref.³⁷ and AMSB models with bilinear R-parity violation have been shown to have testable signatures at a high energy e^+e^- linear collider from the associated production of charged higgs and sleptons.³⁸

4. Signals of AMSB in $e^-\gamma$ and $\gamma\gamma$ Collider

In Ref. ³⁹, the process $e^-\gamma \rightarrow \tilde{\nu}\tilde{\chi}_1^-$ was considered to look for signals of AMSB. Once produced, the sneutrino may decay into either an $(e^-\tilde{\chi}_1^+)$ pair or a $(\nu\tilde{\chi}_1^0)$ pair. Concentrating upon the former, we are left with a fast e^- (which serves as the trigger), two heavily ionizing charged tracks coming from the long-lived $\tilde{\chi}_1^\pm$ and/or two visible soft pions with opposite charges and a large missing transverse momentum (\cancel{p}_T). This is a very unique and distinct signature of anomaly mediated supersymmetry breaking and does not readily arise in either of mSUGRA or GMSB scenarios.

It turns out that, for most of the mAMSB parameter space, the two charged pions are well separated from each other. The neutralinos, on the other hand, escape detection, thereby giving rise to an imbalance in momentum.

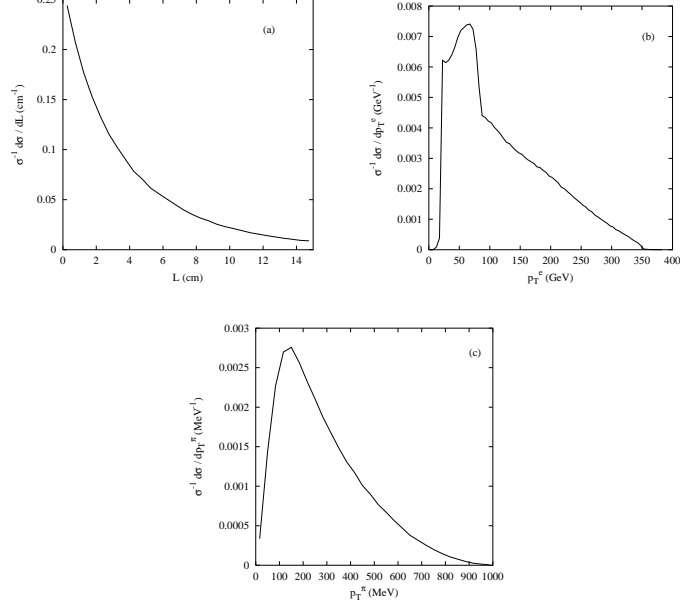


Fig. 1. Normalized kinematic distributions of decay products: (a) decay length of the lighter chargino, (b) p_T of charged lepton, and (c) p_T of the charged pion arising from $e^\pm + \pi^\mp + \cancel{E}_T$ signal for spectrum A. The AMSB input parameters are $m_{3/2} = 44$ TeV, $\tan \beta = 30$, $\mu > 0$ and $m_0 = 410$ GeV.

The signal, then is,

$$e^- \gamma \rightarrow \tilde{\nu}_e \tilde{\chi}_1^- \rightarrow e^- + \pi^+ \pi^- + \cancel{p}_T, \quad (7)$$

with the energetic electron serving as the trigger for the event. The relatively small decay width of the charginos is manifested in heavily ionizing charged tracks (one for each chargino) terminating inside the detector after traversing a macroscopic distance and ending in a soft pion (with $p_T > 200$ MeV) in the Silicon Vertex Detector (SVD) located very close to the beam pipe. The details of the SM backgrounds, selection cuts and the kinematic distributions can be found in Ref. ³⁹.

4.1. Signal strength and the parameter space

Let us now look into the total signal strength as a function of the parameters involved. We shall restrict ourselves to two discrete values of $\tan \beta$ while allowing m_0 and $m_{3/2}$ to vary freely modulo the experimental constraints. As for the beam polarization, we make a particular choice, namely $P_L = +1, P_b = P_{e^-} = -0.8$.

In Fig.2, the results have been displayed for a machine operating at $\sqrt{s_{ee}} = 500$ GeV, in the form of scatter plots for the cross section, after imposing the cuts, in the plane spanned by m_0 and $m_{3/2}$. In each of the individual graphs, the region marked by X corresponds to a chargino mass of less than 86 GeV, thereby falling foul of the ALEPH bound.⁴⁶ The region Y, on the other hand, would correspond

to the $\tilde{\tau}_1$ being the LSP, a possibility not allowed phenomenologically if R -parity is to be conserved.

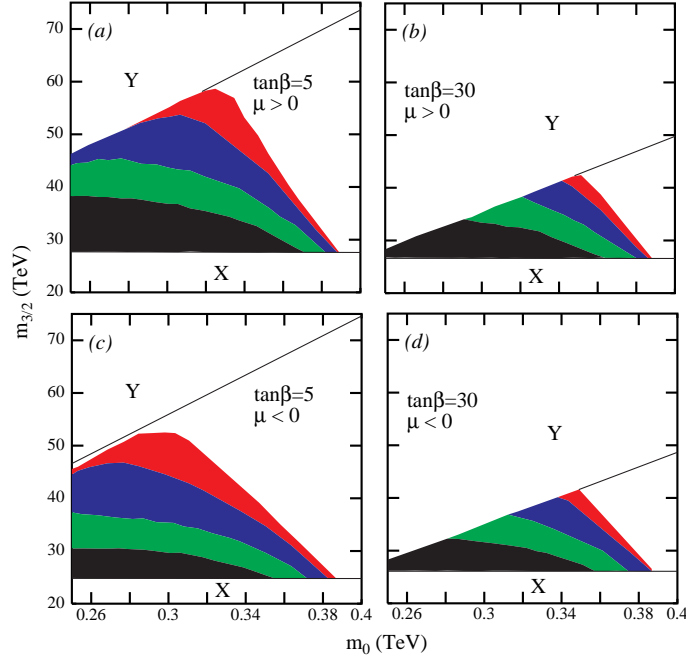


Fig. 2. Scatter plots for the signal cross-section (fb) in the $m_0 - m_{3/2}$ plane for a machine operating at $\sqrt{s_{ee}} = 500$ GeV and $P_L = +1, P_b = P_{e^-} = -0.8$. The values of $\tan\beta$ and $\text{sgn}(\mu)$ are as indicated. The regions marked by X are ruled out by the experimental lower limit on the chargino mass, while those marked by Y are ruled out by the requirement of $\tilde{\chi}_1^0$ being the LSP. In each panel, the top three shaded regions correspond to cross section ranges of $[(0.1 - 5), (5 - 50), (50 - 150)]$. The lowermost region corresponds to $(150 - 470)$ in (a), $(150 - 390)$ in (b), $(150 - 335)$ in (c) and $(150 - 350)$ in (d) respectively. This figure is taken from ³⁹.

It is clear from Fig.2 that, for the low $\tan\beta$ case, an experiment such as this can easily explore $m_{3/2}$ as high as 60(50) TeV for negative (positive) μ . For $\tan\beta = 30$, on the other hand, the maximal reach in $m_{3/2}$ is approximately 40 TeV irrespective of $\text{sgn}(\mu)$. Similarly, the reach in m_0 has little dependence on either of $\tan\beta$ and $\text{sgn}(\mu)$. Finally, it must be borne in mind that Fig.2 has been drawn keeping in mind a moderate luminosity ($\lesssim 100 \text{ fb}^{-1}$). A significantly larger integrated luminosity would, of course, allow one to explore beyond the topmost shaded band. A similar plot for a machine operating at $\sqrt{s_{ee}} = 1$ TeV instead can be seen in Ref. ³⁹. The features are very similar, with the obvious enhancement in the reach.

4.1.1. Parameter determination

The possibility of determining the masses of the chargino and the sneutrino has also been investigated at an $e\gamma$ collider. Since the particles produced were the sneutrino and the chargino and the sneutrino subsequently decayed into a similar chargino

and an electron, it is easy to see that the energy of the decay electron is strictly confined³⁹ within the interval

$$\frac{m_{\tilde{\nu}}^2 - m_{\tilde{\chi}_1^+}^2}{2(E_{\tilde{\nu}}^{\max} + k_{\tilde{\nu}}^{\max})} \leq E^e \leq \frac{m_{\tilde{\nu}}^2 - m_{\tilde{\chi}_1^+}^2}{2(E_{\tilde{\nu}}^{\max} - k_{\tilde{\nu}}^{\max})}, \quad (8)$$

where $E_{\tilde{\nu}}^{\max}$ is the maximum possible energy that the intermediate sneutrino may have carried, viz.

$$E_{\tilde{\nu}}^{\max} = \frac{1}{4y_{\max}\sqrt{s}} \left[(1 + y_{\max}) \left(y_{\max}s + m_{\tilde{\nu}}^2 - m_{\tilde{\chi}_1^+}^2 \right) + (1 - y_{\max}) \sqrt{\left(y_{\max}s + m_{\tilde{\nu}}^2 - m_{\tilde{\chi}_1^+}^2 \right)^2 - 4y_{\max}sm_{\tilde{\nu}}^2} \right], \quad (9)$$

and $k_{\tilde{\nu}}^{\max}$ is the corresponding momentum. y_{\max} is the maximum value of the fraction of the e^{\pm} energy that the reflected photon beam carries off.³⁹

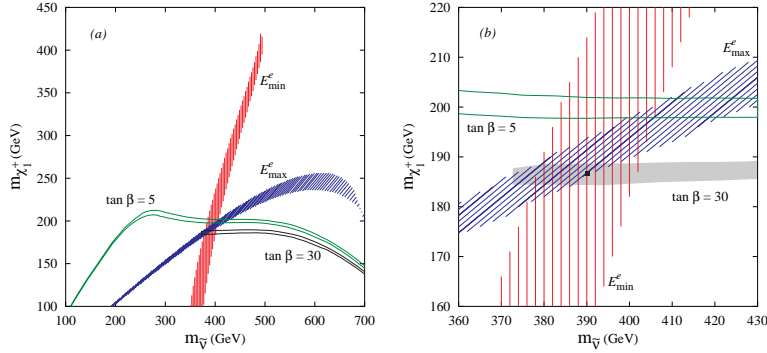


Fig. 3. (a) The determination of the sneutrino and chargino masses from a measurement of the endpoints of the electron energy spectrum (eqn.8). The width of the bands correspond to the error bars in measuring the endpoints.³⁹ For points within the two horizontal bands, the resultant cross section would agree with the measured one to within 1σ . (b) The overlap region has been shown on an expanded scale. The dark square denotes the reference point in the parameter space (pt. **B** in the text). This figure is taken from ³⁹.

As \sqrt{s} and y_{\max} are both known, it follows that an accurate measurement of E_{\max}^e and E_{\min}^e would allow us to determine both the masses. A very precise measurement of the endpoints is unlikely, though. The measurement errors have been discussed in Ref. ³⁹. In Fig. 3a, we display the two bands obtained from the measurement of the two electron energy endpoints corresponding to a particular point in the parameter space ($m_0 = 450$ GeV, $m_{3/2} = 55$ TeV, $\tan \beta = 30$ and $\mu > 0$) leading to $(m_{\tilde{\chi}_1^+}, m_{\tilde{\chi}_1^0}, m_{\tilde{\nu}}) = (186.42, 186.23, 390.07)$ GeV which is denoted as point **B** in Ref. ³⁹. The error on the sneutrino mass, thus determined, is roughly 12 GeV, while that on the chargino mass is roughly 6 GeV. Moreover, the errors are quite correlated (see Fig. 3b, which displays the region of interest on an expanded scale).

Having determined the masses, it is now of interest to measure the remaining parameter, namely $\tan \beta$. Clearly, kinematical distributions are essentially independent of this quantity and one should rather consider cross section measurement. The corresponding error in the cross-section measurement (after imposing the cuts, naturally) is easily determined on application of Poisson (or Gaussian) statistics. Armed with this, and for a given value of $\tan \beta$, one could easily determine the part of the $m_{\tilde{\nu}}-m_{\tilde{\chi}_1^+}$ space that would be consistent with the measured cross-section. In Figs. 3, we display these constraints for two particular values of the ratio $\tan \beta$. Note that, while some resolution is possible, such experiments are not overly sensitive to this parameter. It is possible that significant improvement would occur once other production processes are considered.

4.2. AMSB signals in $\gamma\gamma$ collider

Another possibility of observing AMSB signal is to look for chargino pair production in association with a photon in $\gamma\gamma$ collisions. The production process is solely governed by electromagnetic interactions. The details of the cross sections, selection criteria and background elimination can be found in Ref. ⁴⁰. Assuming an integrated luminosity of 100 fb^{-1} , a chargino mass (considering that the macroscopic track length cannot be seen and the soft charged pions are not observed) up to about 165-170 GeV can be detected at a linear collider operating at $\sqrt{s} = 500 \text{ GeV}$ and the limit can go up to about 370 GeV for a 1 TeV collider. Another important feature of this signal is that just by event counting itself one can have a fairly good determination of $M_{\tilde{\chi}_1^\pm}$.

Before we conclude, it may be relevant to discuss the ways of looking at AMSB signals in the context of the Tevatron or the LHC. It has been shown in Ref. ²⁵ that at the Tevatron one could possibly detect these charginos traveling macroscopic distances and the events can be triggered on high p_T monojets. Production and subsequent decays of other sparticles have also been suggested for triggering on the events. ²⁶ At the LHC, one could look at leptons + jets + charged track + missing energy final states from the sparticle cascades ^{29,30,32} or forward jets + missing energy or one lepton + forward jets + missing energy from gauge boson fusion. ^{31,33} As we have emphasized in this review the soft charged pions might play an important role in looking for signals of AMSB in linear colliders. In a hadronic environment it is almost impossible to look for these soft charged pions with characteristic momentum distribution. Thus, in some sense the searches carried out in linear colliders along the direction discussed in this review can be complementary to the searches in the hadron colliders. Another important aspect is the measurement of the chargino and slepton masses from the kinematics as well as from the cross-section measurements which can possibly identify the underlying model. These measurements may not be very reliable at a hadron collider.

5. Concluding remarks

Anomaly mediated supersymmetry breaking is an interesting way of generating slepton and gaugino masses. At low energies it is beset with tachyonic sleptons. This problem is solved in various ways; here we discuss the minimal model where a constant term m_0^2 is added to all the squared masses of the scalars. Many interesting signatures can be seen in future linear colliders. One interesting feature of AMSB models is that the lighter chargino is winolike (nearly mass-degenerate with the winolike lightest neutralino) and its dominant decay mode is $\tilde{\chi}_1^\pm \rightarrow \tilde{\chi}_1^0 + \text{soft } \pi^\pm$. Fast e^- or ISR photon trigger, heavily ionizing charged track from the slow decay of the lighter chargino and/or soft charged pion with impact parameter resolved can be a distinct possibility in an e^+e^- linear collider. In an $e^-\gamma$ collider one could observe two soft charged pions and two heavily ionizing charged tracks with an e^- trigger whereas in a $\gamma\gamma$ collider one can observe a single photon plus missing energy signal as a test of AMSB. A measurement of the fundamental supersymmetry breaking parameters could also be possible.

Acknowledgments

I am grateful to U. Chattopadhyay, D. Choudhury, E. Gabrielli, D.K. Ghosh, K. Huitu, A. Kundu and P. Roy for collaboration in various works summarised in this review. I would like to thank the Lady Davis Fellowship Trust in Technion for financial support while this work was in progress. Thanks are due to A. Datta and B. Mukhopadhyaya for very useful discussions. This work was supported by the Academy of Finland (project number 48787).

References

1. S. Dimopoulos and H. Georgi, Nucl. Phys. **B193**, 150 (1981) .
2. H.P. Nilles, Phys. Rep. **110**, 1 (1984) .
3. G.F. Giudice and R. Rattazzi, Phys. Rep. **322**, 419 (1999) ; **322**, 501(1999).
4. L. Randall and R. Sundrum, Nucl. Phys. **B557**, 79 (1999) .
5. G.F. Giudice, M.A. Luty, H. Murayama and R. Rattazzi, J. High Energy Phys. **12**, 027 (1998).
6. J.A. Bagger, T. Moroi and E. Poppitz, J. High Energy Phys. **04**, 009 (2000).
7. A. Pomarol and R. Rattazzi, J. High Energy Phys. **05**, 013 (1999);
8. G.D. Kribs, Phys. Rev. D **62**, 015008 (2000) .
9. E. Katz, Y. Shadmi and Y. Shirman, J. High Energy Phys. **08**, 015 (1999).
10. I. Jack and D.R.T. Jones, Phys. Lett. **B482**, 167 (2000).
11. M. Carena, K. Huitu and T. Kobayashi, Nucl. Phys. **B592**, 164 (2000).
12. Z. Chacko, M.A. Luty, I. Maksymyk and E. Ponton, J. High Energy Phys. **04**, 001 (2000).
13. B.C. Allanach and A. Dedes, J. High Energy Phys. **06**, 017 (2000).
14. Z. Chacko, M.A. Luty, E. Ponton, Y. Shadmi and Y. Shirman, Phys. Rev. D **64**, 055009 (2001) .
15. I. Jack and D.R.T. Jones, Phys. Lett. **B491**, 151 (2000).
16. D.E. Kaplan and G.D. Kribs, J. High Energy Phys. **09**, 048 (2000).

17. Z. Chacko and M. Luty, J. High Energy Phys. **05**, 047 (2002); A.E. Nelson and N. Weiner, Phys. Rev. Lett. **88**, 231802 (2002).
18. F. de Campos, M.A. Díaz, O.J.P. Éboli, M.B. Magro and P.G. Mercadante, Nucl. Phys. **B623**, 47 (2002).
19. A. Anisimov, M. Dine, M. Graesser and S. Thomas, Phys. Rev. D **65**, 105011 (2002) ; J. High Energy Phys. **03**, 036 (2002).
20. M.A. Luty and R. Sundrum, Phys. Rev. D **65**, 066004 (2002) ; Phys. Rev. D **67**, 045007 (2003) .
21. R. Harnik, H. Murayama and A. Pierce, J. High Energy Phys. **08**, 034 (2002).
22. I. Jack, D.R.T. Jones and R. Wild, Phys. Lett. **B535**, 193 (2002).
23. B. Murakami and J.D. Wells, Phys. Rev. D **68**, 035006 (2003) .
24. R. Rattazzi, A. Strumia and J.D. Wells, Nucl. Phys. **B576**, 3 (2000).
25. J.L. Feng, T. Moroi, L. Randall, M. Strassler and S. Su, Phys. Rev. Lett. **83**, 1731 (1999) .
26. T. Gherghetta, G.F. Giudice and J.D. Wells, Nucl. Phys. **B559**, 27 (1999) .
27. J.L. Feng and T. Moroi, Phys. Rev. D **61**, 095004 (2000) .
28. S. Su, Nucl. Phys. **B573**, 87 (2000).
29. F. Paige and J. Wells, hep-ph/0001249.
30. H. Baer, J.K. Mizukoshi and X. Tata, Phys. Lett. **B488**, 367 (2000).
31. A. Datta, P. Konar and B. Mukhopadhyaya, Phys. Rev. Lett. **88**, 181802 (2002).
32. A.J. Barr, C.G. Lester, M.A. Parker, B.C. Allanach, P. Richardson, J. High Energy Phys. **03**, 045 (2003).
33. A. Datta and K. Huitu, Phys. Rev. D **67**, 115006 (2003) .
34. A. Datta and S. Maity, Phys. Lett. **B513**, 130 (2001).
35. D.K. Ghosh, P. Roy and S. Roy, J. High Energy Phys. **08**, 031 (2000).
36. D.K. Ghosh, A. Kundu, P. Roy and S. Roy, Phys. Rev. D **64**, 115001 (2001) (Erratum in preparation).
37. K. Choi, K. Hwang and W.Y. Song, Phys. Rev. Lett. **88**, 141801 (2002).
38. M.A. Díaz, R.A. Lineros and M.A. Rivera, Phys. Rev. D **67**, 115004 (2003) .
39. D. Choudhury, D.K. Ghosh and S. Roy, Nucl. Phys. **B646**, 3 (2002).
40. D. Choudhury, B. Mukhopadhyaya, S. Rakshit and A. Datta, J. High Energy Phys. **01**, 069 (2003).
41. H.C. Cheng, B.A. Dobrescu, K.T. Matchev, Nucl. Phys. **B543**, 47 (1999) .
42. C.H. Chen, M. Drees, and J.F. Gunion, Phys. Rev. Lett. **76**, 2002 (1996) ; Phys. Rev. D **55**, 330 (1997) ; Phys. Rev. Lett. **82**, 3192(E) (1999) ; J.F. Gunion and S. Mrenna, Phys. Rev. D **64**, 075002 (2001) .
43. U. Chattopadhyay, D.K. Ghosh and S. Roy, Phys. Rev. D **62**, 115001 (2000) .
44. K. Huitu, J. Laamanen, P.N. Pandita, Phys. Rev. D **65**, 115003 (2002) .
45. DELPHI Collaboration, M. Elsing, available from http://www.cern.ch/~offline/physics_links/lepc.html
46. ALEPH Collaboration, A. Heister *et al.*, hep-ex/0203020.
47. J.L. Feng and K.T. Matchev, Phys. Rev. Lett. **86**, 3480 (2001); K. Choi, K. Hwang, S.K. Kang, K.Y. Lee, and W.Y. Song, Phys. Rev. D **64**, 055001 (2001) .
48. U. Chattopadhyay and P. Nath, Phys. Rev. Lett. **86**, 5854 (2001); H. Baer, C. Balazs, J. Ferrandis, X. Tata, Phys. Rev. D **64**, 035004 (2001) ; K. Enqvist, E. Gabrielli, K. Huitu, Phys. Lett. **B512**, 107 (2001).
49. A. Datta, A. Kundu and A. Samanta, Phys. Rev. D **64**, 095016 (2001) .
50. E. Gabrielli, K. Huitu and S. Roy, Phys. Rev. D **65**, 075005 (2002) .
51. A. García-Bellido, Nucl. Phys. **B** (Proc. Suppl.) **109B** 236 (2002).
52. T. Alderweireld, hep-ex/0205053.